FULL PAPER

Dielectric Relaxation Processes, Electronic Structure, and Band Gap Engineering of MFU-4-type Metal-Organic Frameworks: Towards a Rational Design of Semiconducting Microporous Materials

Pit Sippel, Dmytro Denysenko, Alois Loidl, Peter Lunkenheimer, German Sastre,* and Dirk Volkmer*

The electronic structures and band gaps of MFU-4-type metal-organic frameworks can be systematically engineered leading to a family of isostructural microporous solids. Electrical properties of the microcrystalline samples are investigated by temperature-dependent broad-band dielectric and optical spectroscopy, which are corroborated by full band structure calculations performed for framework and cluster model compounds at multiple levels of density functional theory. The combined results glean a detailed picture of relative shifts and dispersion of molecular orbitals when going from zero-dimensional clusters to three-dimensional periodic solids, thus allowing to develop guidelines for tailoring the electronic properties of this class of semiconducting microporous solids via a versatile building block approach. Thus, engineering of the band gap in MFU-4 type compounds can be achieved by adjusting the degree of conjugation of the organic ligand or by choosing an appropriate metal whose partially occupied d-orbitals generate bands below the LUMO energy of the ligand which, for example, is accomplished by octahedral Co(II) ions in Co-MFU-4.

1. Introduction

Metal-organic frameworks (MOFs) represent a particular class of coordination polymers which possess crystalline periodic structures and retain permanent porosity upon loss of solvent molecules occluded in the crystal lattice during synthesis. Empirical construction rules have been developed during the last some 20 years, enabling scientists to build-up quite successfully an ever-increasing number of topologically different frameworks solids. However, to go beyond crystal engineering, that is, to engineer their electronic properties for implementing MOFs in electronic devices,[1] photochemistry,[2] or clean energy applications,[3] a detailed analysis of their electronic band structures becomes necessary, a challenge which as yet has attracted much less attention by the scientific community. Notable exceptions include frameworks derived from the MOF-5[4] family of compounds, for which the electronic structure of the parent compound itself has been analyzed in great detail by quantum mechanical calculations.[5] Recent work has covered the influence of isostructural substitution of different building units in MOF-5-type compounds (Zn vs Co,[6] Cd, Be, Mg, and Ca,[7] O^{2-} vs S^{2-}, Se^{2-}[8], including in-depth studies on the influence of the organic dicarboxylate linkers on the band structure of the resulting solids,[9] and screening of combinatorial substitutions (metal ions, linkers).[10] Similar combined theoretical and spectroscopic investigations were also reported for UiO-66.[11] Only very few experimental studies have been so far devoted to the electrical conductivity of metal-organic frameworks,[12] which, however, were not complemented by theoretical studies, in contrast to covalent-organic frameworks (COFs) and π-stacked self-organized organic solids, the electrical conductivity and charge carrier mobility of which have been measured and analyzed by theoretical approaches.[13]

Metal-organic frameworks inherit both characteristic properties of molecular as well as ionic solids, which results from their structural building units comprising small (charged) organic molecules (= ligands or linkers) and (transition) metal ions. Merging both components into three-dimensional periodic solids, a (moderate) spreading and shift of electron energy levels thus is expected, compared to the corresponding zero-dimensional building units.

Intended as case study, we here present combined investigations on the dielectric properties, dc-/ac-electrical conductivity,

P. Sippel, Prof. A. Loidl, Dr. P. Lunkenheimer
Chair of Experimental Physics V
Center for Electronic Correlations and Magnetism
University of Augsburg
Universitätsstr. 2
D-86135 Augsburg, Germany

D. Denysenko, Prof. D. Volkmer
Chair of Solid State and Material Science
Institute of Physics
University of Augsburg
Universitätsstr. 1, D-86135 Augsburg, Germany
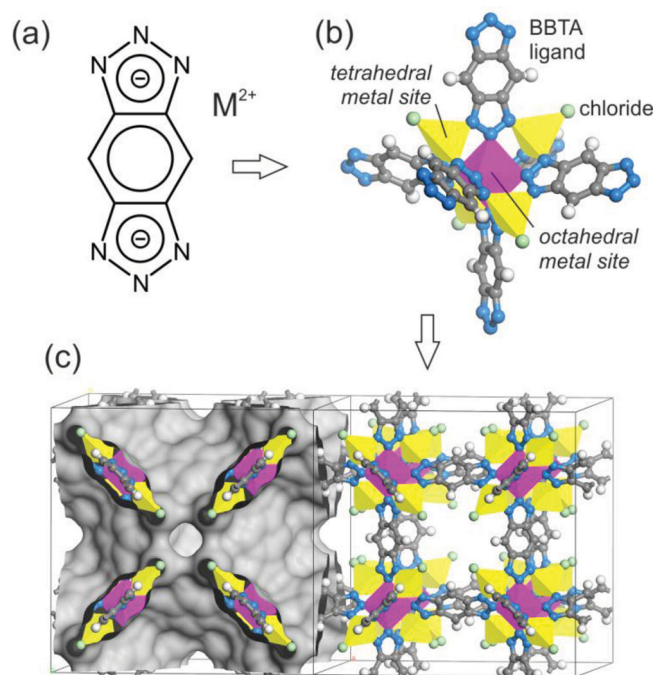E-mail: dirk.volkmer@physik.uni-augsburg.de

Dr. G. Sastre
Instituto de Tecnologia Quimica (UPV-CSIC)
Universidad Politecnica de Valencia
Av. Los Naranjos s/n
46022 Valencia, Spain

FULL PAPER

and optical/electronic band gaps of the metal-organic frameworks MFU-4,[14] and Co-MFU-4,[15] which are gleaned from spectroscopic and quantum mechanical methods. MFU-4-type frameworks[16] possess unique structural features that render them attractive candidates for developing novel semiconductors which combine structural and chemical robustness, high porosity (specific surface area values typically exceeding 1000 m^2 g^{-1}), thermal stability up to 350 °C in air and 500 °C in inert atmosphere, stability against moisture under ambient conditions, and options for a systematic fine adjustment of electronic properties, that is, matching of the Fermi energy level, electronic and optical band gap, and conductivity.

The parent compound MFU-4 (Metal-Organic Framework Ulm-University-4) crystallizes in a cubic lattice, within space group $Fm(1)m$ (no. 225), a = 21.697(3) Å. The framework is composed of so-called Kuratowski-type coordination units, which are cross-linked into three dimensions (**Figure 1**).[17] Substituting all Zn^{2+} by Co^{2+} ions leads to Co-MFU-4, which—based on atom positions and crystallographic symmetry—is isostructural with MFU-4. Introducing paramagnetic cobalt centers into this framework, however, leads to dramatic changes of the framework's electronic properties, as revealed by different spectroscopic techniques. Note that the formal subdivision of metal-organic frameworks into secondary building units (SBUs) such as those shown in Figure 1, is different to the conventions in zeolite science,[18] but can be justified on the base of DFT calculations as will be shown in the following. Freshly prepared MFU-4 (Co-MFU-4, resp.) contains

N,N-dimethylformamide (DMF) solvent molecules, which are occluded in the large voids of the framework (the fraction of void volume of the unit cell is about 58%). Each cubic unit cell of MFU-4 contains 4 almost spherical cavities with an approx. diameter of ca. 12 Å. Based on the results from thermogravimetric analysis (TGA) each of these encloses up to six DMF molecules (**Figure 2**),[14] which can be completely removed if the sample is heated up to T = 320 °C and kept for 16 h in high-vacuum (p = 0.1 mbar).

Employing dielectric spectroscopy performed at temperatures between 10 and 600 K, a variety of relaxation processes is detected in both materials. They can be ascribed to reorientational motions of dipolar (solvent) molecules trapped within the pores of the metal-organic framework, suggesting MFU-4 as an interesting material for testing molecular dynamics in confined environment. Dielectric spectroscopy applied to MOFs[19] is an excellent analytical technique to probe the residual amount of occluded solvent molecules, which remains in the porous framework upon heat treatment/evacuation. Knowing and controlling the total amount of occluded solvent molecules is a crucial requirement for quantitative studies of the frameworks' electronic properties, especially if a quantitative comparison to results from quantum mechanical calculations is intended. In addition, dielectric measurements on the pure frameworks (i.e., all solvent molecules being removed) reveal information on the dc conductivity of these materials, reaching values as low as 10^{-14} Ω^{-1} cm^{-1}. Its temperature dependence shows thermally activated behaviour and the energy barriers determining the charge transport were deduced for both materials. These results are compared to the gap energies as revealed by diffusive UV/VIS/NIR reflectance spectroscopy and full band structure calculations employing plane-wave DFT with GGA and hybrid functionals (PBE, HSE). Band conduction with an energy barrier of the order of 3 eV is the dominating charge transport process for MFU-4. In contrast, in Co-MFU-4 the situation is more complex and hopping conductivity of localized electrons seems to play an important role in this material. Both results are discussed with respect to results from quantum mechanical calculations, thus leading to guidelines for tailoring electronic properties of this class of semiconducting microporous solids via a building block approach.

2. Results and Discussion

2.1. Relaxation Dynamics

Frequency dependent dielectric measurements employing a capacitor cell (Experimental Section) were performed on powder samples of MFU-4 which have been subjected to different pretreatment conditions. **Figure 3** shows the temperature dependence of the dielectric constant ε' and the real part of the conductivity σ' of MFU-4 for various measurement frequencies. The curves shown have been collected in two separate measurement runs, below and above room temperature, with a new preparation of the sample capacitor before each run. Obviously, the two sets of conductivity curves do not perfectly match at 300 K. This demonstrates the dependence of σ' on sample history (especially, pressure and moisture), despite

Figure 1. Stepwise assembly of MFU-4-type frameworks from different building units: a) metal ions (M) and benzo[1,2-d:4,5-d']bis([1,2,3]triazolate (BBTA^{2-}) linkers; b) [M$_5$Cl$_4$(BBTA)$_6$], a Kuratowski-type secondary building unit; c) MFU-4 crystal model showing two unit cells, one of which includes the 3d model of a Connolly surface, calculated for a solvent probe radius of 1.2 Å.
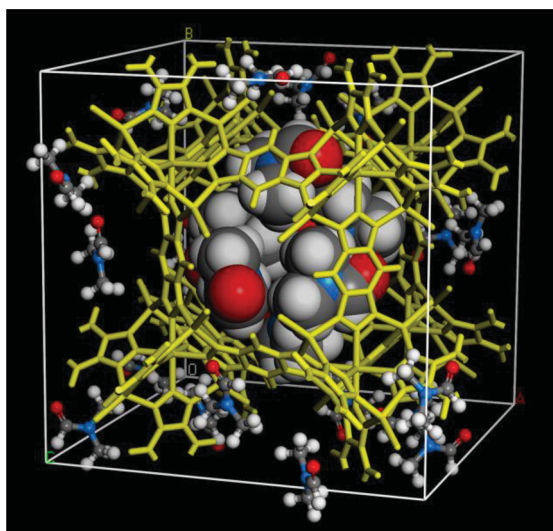
www.MaterialsViews.com

ADVANCED
FUNCTIONAL
MATERIALS
www.afm-journal.de

FULL PAPER

Figure 2. Packing plot of a wire model of MFU-4 (yellow), in which internal voids are filled with *N*,*N*-dimethylformamide (DMF) solvent molecules. The cubic face-centered unit cell contains four almost spherical cavities holding up to 24 DMF molecules in total, which become occluded during synthesis. For clarity only those 6 DMF molecules are high-lighted as CPK models which are located in the central cavity. (DMF: C, grey; N, blue; H, white; O, red).
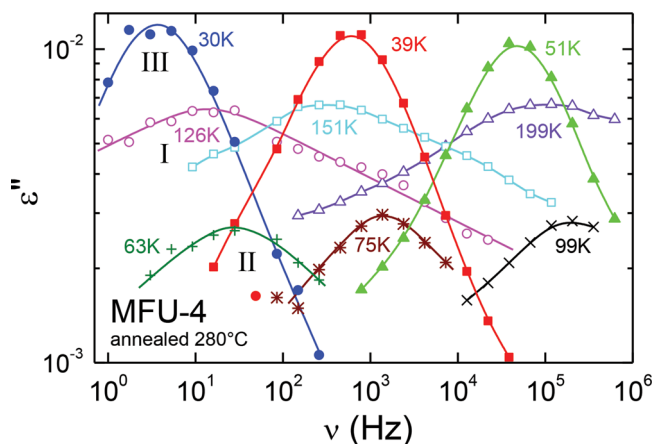

Figure 3. Temperature dependence of a) the dielectric constant and b) conductivity of MFU-4 heated at 280 °C in vacuum, measured at various frequencies. The inset shows a magnified view of $\varepsilon'(T)$ in the region below room temperature for selected frequencies. In the low-temperature region, three relaxation processes are revealed, denoted as I–III.

both samples have been subjected to vacuum before the measurement for the same period of time (see experimental section). At low temperatures, $\varepsilon'(T)$ (Figure 3a) is of the order of 2 and nearly temperature and frequency independent (less than 10% variation). The dielectric constant in this region can be assumed to mainly arise from the ionic and electronic polarizability, i.e., it represents the quantity usually termed ε_∞. However, as shown in the inset of Figure 3, at least two small successive steps in $\varepsilon'(T)$ are superimposed to this constant value. They shift to higher temperatures with increasing frequency, thus showing the typical signature of relaxation processes.[20] The step-like behavior of $\varepsilon'(T)$ can be ascribed to the fact that, for a given frequency, the relaxing entities can no longer follow the ac field when temperature is lowered. At high temperatures, $T > 400$ K, a strong, frequency-dependent increase of ε' is found, which also may represent contributions from relaxational response and/or from hopping conductivity ($\varepsilon' \propto \nu^{s-1}$ with $s < 1$).[21]

In $\sigma'(T)$ (Figure 3b), a number of peaks and shoulders show up (the most pronounced ones observed in the low-temperature region are marked by I–III), which shift to higher temperatures with increasing frequency.[22] Again, this behavior is typical for relaxation processes.[20] In $\varepsilon'(T)$, corresponding steps are expected, with their points of inflection occurring at the peak positions in $\sigma'(T)$. As mentioned above, for the lower temperatures these relaxation steps are shown in the inset of Figure 3. At the peak, the measurement frequency is related to the relaxation time via $2\pi\nu = 1/\tau$. As the relaxation time characterizes the dynamics of the relaxing entities, for thermally activated processes τ should decrease with increasing temperature. This explains the observed shift of the relaxation peaks (and steps in ε') with frequency.
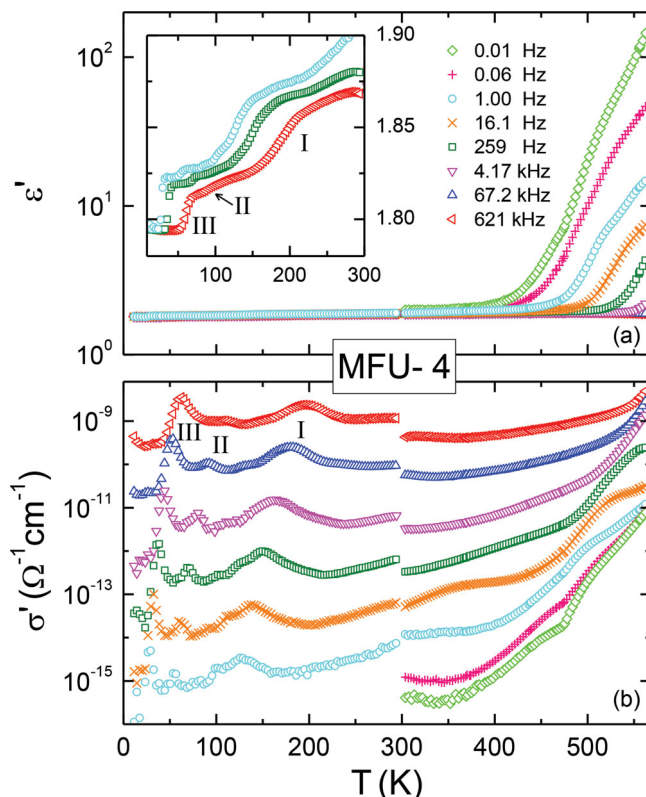
In **Figure 4** the frequency dependence of the dielectric loss is shown for the same sample. The spectra measured at various temperatures below 200 K reveal peaks that arise from the same relaxation processes as the corresponding peaks in Figure 3, marked by I–III. Again, at the peak position the relation $2\pi\nu = 1/\tau$ applies. In this temperature region, three

Figure 4. Frequency dependence of the dielectric loss of MFU-4 (heated at 280 °C in vacuum) as measured at selected temperatures. The lines are guides for the eyes. Three relaxation processes are revealed, corresponding to those labeled I–III in Figure 3.

ADVANCED
FUNCTIONAL
MATERIALS
www.afm-journal.de

Materials
Views
www.MaterialsViews.com

separate relaxation processes show up: The peaks at 199, 151, and 126 K correspond to process I, observed between 100 and 200 K in Figure 3b. Their strong shift to lower frequencies directly mirrors the slowing down of the relaxation dynamics when temperature is lowered. Below about 120 K, this peak shifts out of the frequency window and a second process shifts in from high frequencies, which explains the observed peaks at 99, 75, and 63 K. It is related to the small maxima denoted as process II in Figure 3b. Finally, at even lower temperatures, a third peak enters the frequency window (30, 39, and 51 K). It corresponds to the strongest process, denoted as III, observed at the lowest temperatures in Figure 3b.

Generally, spectral signatures of relaxations as revealed in Figures 3,4 can arise from different phenomena.[20,23,24] Intrinsic relaxation processes usually involve the reorientation of dipolar entities. These entities can be dipolar molecules, for example, in liquids and supercooled liquids like water or glycerol.[23] In some crystalline materials (sometimes termed "plastic crystals") molecular reorientations are possible, too,[25] a prominent example being Buckminster fullerene (C_{60}).[26] In addition, intramolecular degrees of freedom, involving the reorientation of a dipolar moment, can also lead to relaxation features in dielectric spectra. Well-known examples are the side group motions of polymers.[27] In the present case of MFU-4, one may suspect that residual amounts of the solvent DMF, used during sample synthesis, or of absorbed water are located within the cages formed by the metal-organic framework. These dipolar molecules, whose reorientation may be influenced by interactions with the cage walls or other absorbed molecules, can be assumed to lead to at least some of the observed relaxation features revealed by Figures 3,4.

To check for this notion, we have performed additional dielectric measurements of a MFU-4 sample, for which the DMF solvent was not removed after sample synthesis and for a sample heated under vacuum at higher temperature of 320 °C instead of 280 °C. (Measurements were performed both under cooling and heating, revealing no significant difference of both runs. Thus a variation of the DMF content during the dielectric characterization can be excluded. In **Figure 5**, only the heating results are shown to avoid overcrowding of the figure.) Figure 5 compares the $\varepsilon'(T)$ and $\varepsilon''(T)$ results for the three samples at temperatures below 300 K and selected frequencies. Indeed, as can best be seen in $\varepsilon''(T)$ shown in Figure 5b, relaxation process I is most pronounced in the sample containing large amounts of DMF. Its amplitude is strongly reduced by about a factor of 10 for the sample heated at 280 °C and it is completely suppressed in the sample kept at 320 °C. This finding clearly points to a solvent-related origin of at least one of the observed relaxations, which in the 280 °C sample can be ascribed to minor residual amounts of DMF. However, it should also be noted that the rather sharp relaxation peaks arising in the region around 50 K in the sample heated at 280 °C (peak III in Figure 5b), are much weaker or even absent in both the non-treated sample and the sample annealed at a higher temperature. Moreover, the non-treated sample exhibits another high-temperature peak of unknown origin (e.g., at 200 K for 1 Hz), not detected in the other samples.

The maximum number of DMF molecules that can reside in a pore of the MFU-4 structure is six,[14] which should be the
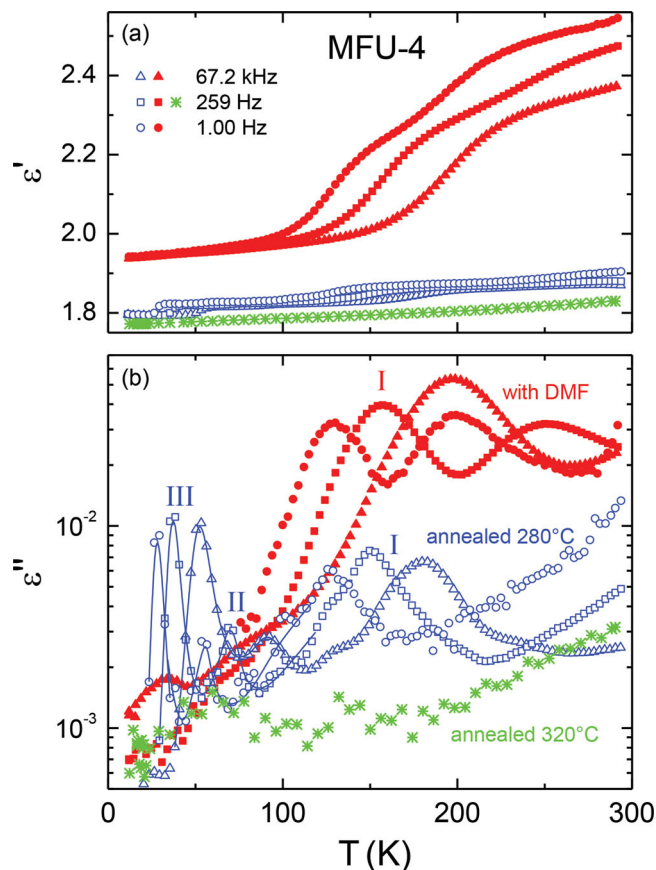
Figure 5. Temperature dependence of a) the dielectric constant and b) loss at various measurement frequencies. The open symbols show the results for a MFU-4 sample, for which the DMF solvent was removed at 280 °C (data from the same measurement are also shown in Figures 3,4), while the stars show the results for the sample subjected to 320 °C. For clarity, for the latter only data at a single frequency are shown. The closed symbols were obtained for a sample prepared without removing the DMF. The lines in (b) are guides for the eyes.

case for the non-treated sample. However, in the sample heated at 280 °C, also cases should occur where the number of DMF molecules per pore is smaller. Thus, the additional relaxations II and III, observed in this sample at lower temperatures (i.e., faster relaxation rates) than process I, can be assumed to be due to pores filled with a smaller number of molecules, leading to less restricted reorientational motions. In **Figure 6**, we present the relaxation map of this sample. $\tau(T)$ as determined from the peak positions in Figures 3,4 is shown in Arrhenius representation, which should lead to linear behavior for thermally activated motions according to the Arrhenius law, $\tau = \tau_0 \exp[E/(k_B T)]$ (τ_0 is an inverse attempt frequency and E represents the activation energy). Indeed, reasonable linear fits are possible for processes I–III. From their slopes, energy barriers of 0.40 eV (process I), 0.13 eV (II), and 0.060 eV (III) are deduced.

In addition, in Figure 6 also relaxation times of pure DMF are included, partly taken from literature[28] (248 – 338 K) and partly determined in the present work (173 – 213 K). The latter includes data measured in the supercooled liquid state below the melting point of 213 K. Using cooling rates of up to 0.6 K min⁻¹, supercooling of the bulk material (DMF) was
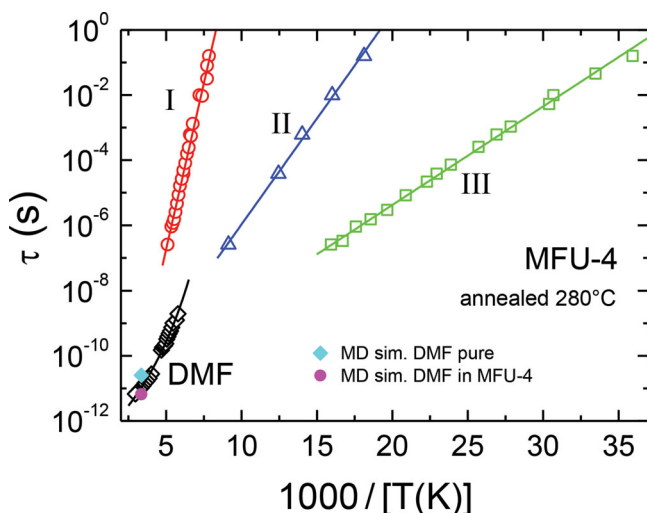
Figure 6. Temperature dependence of relaxation times of the three fastest processes (I–III) in MFU-4 annealed at 280 °C (circles, triangles, and squares). The lines are linear fits. Diamonds show the relaxation times of liquid and supercooled DMF. The data in the liquid state at $1000/T < 4.5$ K^{-1} were taken from ref. [28]. The line shows a fit with the Vogel-Fulcher-Tammann (VFT) function ($\tau_0 = 1.8 \times 10^{-13}$ s, $D = 11.8$, $T_{VF} = 76.5$ K). The solid symbols show τ at 298 K of pure DMF and of DMF loaded in MFU-4 as obtained from MD simulations.

possible down to 173 K while below this temperature crystallization occurred. The line through the data points is a fit with the modified Vogel-Fulcher-Tammann (VFT) law, $\tau = \tau_0 \exp[D\, T_{VF}/(T - T_{VF})]$, where D is the so-called strength parameter and T_{VF} is the Vogel-Fulcher temperature.[29,30] This empirical law is often used to parameterize relaxation-time data in liquids and supercooled liquids.[23] Phenomenologically, the super-Arrhenius behavior as described by the VFT law can be thought to result from a temperature-dependent energy barrier.

It becomes obvious from Figure 6 that none of the relaxations found in MFU-4 provides a reasonable continuation of the relaxation time curve of DMF. To explain this finding, we suggest that peak I corresponds to the case of six molecules per cage. For this maximum pore filling, the relaxation is considerably slowed down due to sterical hindering of reorientational motion compared to pure DMF. Processes II and III can be assumed to be due to cases of a smaller number of DMF molecules per pore, which leads to faster relaxation due to a less dense packing of the DMF molecules in the pores. Processes II and III seem to be faster than the reorientational motion in pure DMF, estimated by an extrapolation of the VFT curve in Figure 6. Such an acceleration of relaxations in confined geometry is a well-known effect, occurring when exchange interactions with the pore wall can be neglected.[31] It mirrors the fact that in most liquids, it is the interaction between individual molecules that make relaxation processes slow and in fact it is the growing correlation length scale that finally leads to the glass transition at low temperatures in many liquids.[32] In the fully packed pores of the non-treated sample, the relaxation may be sterically hindered but in the less densely packed cases, the reduced correlations due to the reduction of the number of next neighbors, compared to the bulk, comes into effect and

leads to an acceleration of reorientational motion. It should be noted that relaxations II and III closely follow Arrhenius behavior (Figure 6), in marked contrast to the non-Arrhenius $\tau(T)$ curves of bulk DMF. Remarkably this is just what was found in various experiments on confined liquids, where deep in the supercooled state a transition to Arrhenius temperature dependence of $\tau(T)$ was reported.[31] This was ascribed to single-molecules dynamics with strongly reduced cooperativity arising from the confinement.

The dynamic electrical poling behavior of DMF-loaded MFU-4 was also examined by molecular dynamics (MD) simulations (see Supporting Information for technical details), which glean further support to the assumption that the relaxation processes observed in dielectric spectroscopy experiments are due to the (rotational) motion of occluded DMF molecules, responding to the applied external electric field. Since computational modeling of the dynamic behavior of solvent-loaded MFU-4 was much simpler to implement in time than in frequency domain, a series of force field based MD trajectories were recorded in order to glean an atomistic picture of the electrical poling process.[33] Briefly, periodic box models containing atomic ensembles of pure DMF, MFU-4, and DMF-loaded MFU-4 were subjected to a constant electrical field, which was applied in z-direction. Upon switching off the field, the depolarization of the simulation box with time was sampled at constant temperature (298 K) and constant volume or pressure (1 atm). Representative traces of the time-dependent changes of the z-component of the simulation cells' dipole moments are shown in **Figure 7**.

Employing non-linear regression analysis, the relaxation data shown in Figure 7 were fitted as single exponential decays (function: $y_0 + A\, e^{(-t/\tau)}$) yielding characteristic decay time constants of $\tau = 6.6$ ps for DMF@MFU-4, and $\tau = 25.3$ ps for pure DMF. The corresponding relaxation data of the MFU-4 framework without DMF, in contrast, showed a much faster depolarization (Figure 7, inset) which could not be fitted by a single exponential decay. Time and frequency-domain data are directly related via Fourier transformation and, thus, the relaxation times obtained from their analysis can be directly compared.
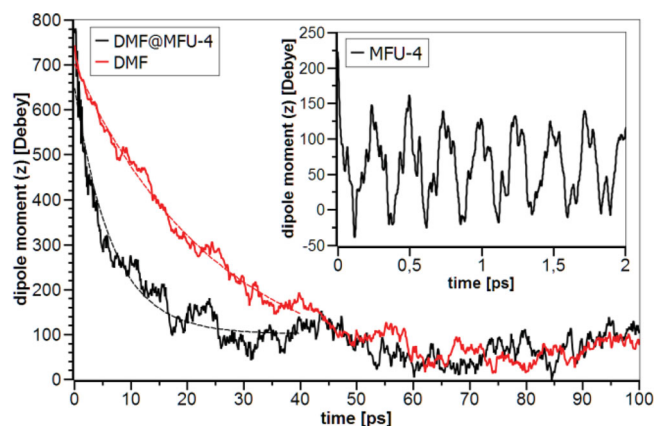

Figure 7. Time-dependent depolarization curves derived from atomistic MD runs of periodic boxes containing pure DMF molecules (red curve), or DMF-loaded MFU-4 (black curve) sampled at 298 K (UFF force field). The inset shows the corresponding data for MFU-4 without DMF. (Note the largely different time scales for the latter MD run. Technical details of the simulations are given in the Supporting Informations).

**ADVANCED
FUNCTIONAL
MATERIALS**

www.afm-journal.de

*Materials
Views*

www.MaterialsViews.com

The time constants at 298 K, derived for DMF from the time-dependent depolarization curves of Figure 7, are shown as closed symbols in Figure 6. Obviously, both values of τ are of similar order of magnitude as those obtained from dielectric spectroscopy for pure DMF and also for occluded DMF if extrapolated to room temperature. Thus, atomistic simulations reveal in a semi-quantitative manner that in fact the experimental relaxation processes observed by dielectric spectroscopy should be ascribed to the dynamic re-orientation of polar solvent molecules in the voids of the framework. Targeting at a quantitative correlation between experimental and simulated values would require a customized force field including a precise adjustment of force-field parameters to suitable reference systems, for the non-bonding interactions in particular, a major task which is clearly beyond the scope of the present studies. In any case, the present results demonstrate that metal-organic frameworks represent promising host systems for the investigation of glass-forming materials under confined geometry. They may serve for the investigation of correlation length scales and also of the supercooled states of materials that cannot be easily supercooled and strongly tend to crystallize in bulk form (e.g., water). In this context, it should be noted that in the present case processes I – III were observed far below the melting point of DMF (213 K), that is, deep in the supercooled state, which seems to be inaccessible for the bulk material.

2.2. Electrical Conductivity and Charge Transport

In **Figure 8**a, we show the conductivity $\sigma'(T)$ of MFU-4 (heated at 280 °C) and Co-MFU-4 for various frequencies. Just as for MFU-4 (cf. Figure 3b), also in Co-MFU-4 several peaks and shoulders show up in $\sigma'(T)$, indicating relaxational behavior. Here we focus on the charge transport properties of these materials. Figure 8a reveals that for comparable frequencies the conductivity of the Co sample is significantly higher than for the pure sample. At the highest temperatures and lowest frequencies investigated, the $\sigma'(T)$ curves in Figure 8a for each material approach each other, that is, the conductivity starts to become frequency independent. Thus, here the measured $\sigma'(T)$ represents the dc conductivity $\sigma_{dc}(T)$. Based on a comparison of the 0.01 Hz and 0.02 Hz curves, the 0.01 Hz curve can be assumed to be a good estimate of the dc conductivity above a temperature of about 480 K for MFU-4 and 420 K for Co-MFU-4. It should be noted that for both systems the dc conductivity is relatively low, reaching values below 10^{-13} Ω^{-1} cm^{-1} for the pure sample, which is far out of the resolution limit of most conventional dc measurement techniques.

For the dc conductivity of semiconductors and insulators, often an Arrhenius law, $\sigma_{dc} \propto \exp[-E/(2\,k_B T)]$, is found, where E represents the energy gap between valence and conduction band. Figure 8b shows an Arrhenius representation of the conductivities at 0.01 Hz at high temperatures, where they represent the dc values. Here a possible Arrhenius temperature dependence of $\sigma_{dc}(T)$ should lead to linear behavior, which for MFU-4 indeed is found. For Co-MFU-4, $\sigma_{dc}(1/T)$ can be described by a straight line below about 500 K only.[34] Towards higher temperatures, the dc conductivity continuously exceeds the Arrhenius behavior. This is expected when in a complex
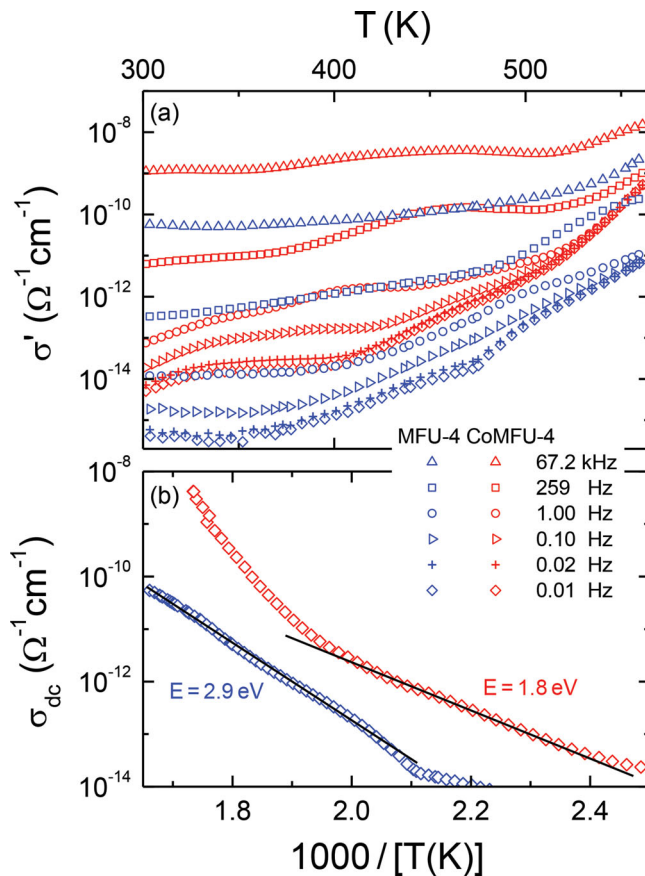

Figure 8. a) Comparison of the temperature-dependent conductivity of MFU-4 (blue) and Co-MFU-4 (red) for various frequencies. b) Conductivity at 0.01 Hz for MFU-4 and Co-MFU-4 in Arrhenius representation (in MFU-4, the measurements were extended up to 600 K in a separate low-frequency measurement). The plot is restricted to the high-temperature region, where σ' at 0.01 Hz provides a reasonable estimate of the dc conductivity. The lines are fits assuming Arrhenius behavior, $\sigma_{dc} \propto \exp[-E/(2k_B T)]$. The resulting energy barriers are noted in the Figure.

band structure an increasing number of direct and indirect transitions become possible at elevated temperatures. Thus it seems reasonable that the linear region of the dc conductivity below about 500 K is dominated by the intrinsic band gap. The lines in Figure 8b represent fits by the Arrhenius law, revealing energy barriers of 2.9 eV for the pure system and 1.8 eV for Co-MFU-4.

2.3. Optical Band Gaps

The absorption coefficient α is related to the measured diffusive reflectance R via the Kubelka-Munk function: $F_{KM} = \alpha/s = (1-R)^2/2R$, where s is the scattering coefficient. **Figure 9** shows plots of F_{KM} of MFU-4 and Co-MFU-4 at room temperature, allowing to estimate a band gap value of 3.05 eV (MFU-4) and 1.84 eV (or 2.72 eV; see discussion below) (Co-MFU-4). A more detailed band gap analysis was performed using so-called Tauc plots of the spectral data.[35] Within this approach, the absorption coefficient α should be related to the band gap energy E_g according to the following equation: $\alpha h\nu \propto (h\nu - E_g)^n$,
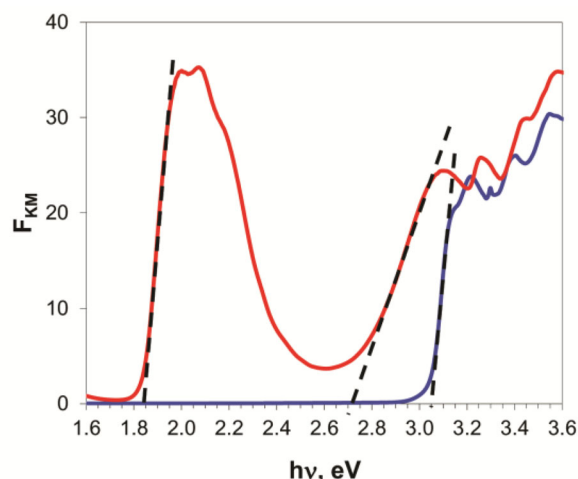
Figure 9. Spectra of F_{KM} of MFU-4 (blue curve) and Co-MFU-4 (red curve) as determined from diffuse UV/vis reflectance measurements sampled at room temperature. The dashed lines demonstrate the cut-off energies, corresponding to the band gap values.

where n is 1/2, 3/2, 2, or 3 for direct allowed, direct forbidden, indirect allowed, or indirect forbidden transitions, respectively. Assuming, that s is independent of wavelengh, the Kubelka-Munk function can be used to prepare Tauc plots (One should be aware that for small band gaps and cases close to single-molecules excitations, it is rather unclear if the use of Tauc plots is justified. However, it seems the only reasonable alternative to a linear extrapolation as shown in Figure 9 and in the present case leads to rather similar results).

Figure 10 shows such plots, corresponding to a representation that should linearize the data in the region of the electronic gap excitation for the case of a direct allowed transition. For MFU-4, a clearly-developed absorption edge shows up with a well-defined linear region, whose extrapolation leads to
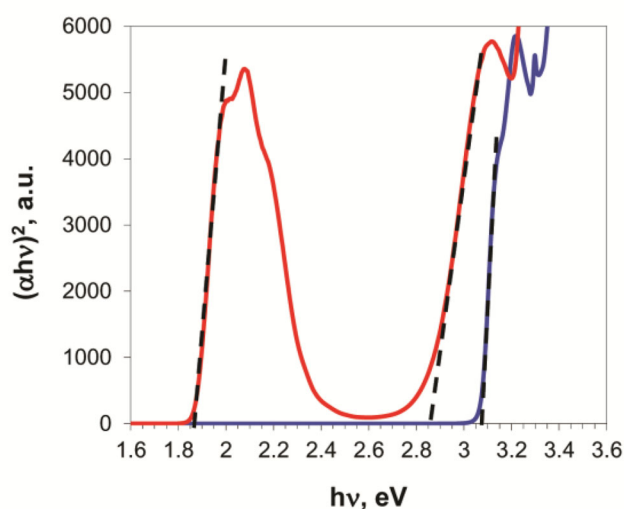
a band gap of about 3.08 eV. It should be noted that we also found reasonable linear behavior in Tauc plots with exponents 2/3, 1/2, and 1/3, and therefore it is difficult to make a statement concerning the validity of the different types of interband transitions. However, all these plots give very similar values of the band gap for MFU-4 ranging from 3.01–3.08 eV, which, moreover, are very close to the value obtained directly from the diffuse reflectance spectrum (Figure 9). The resulting band gap of 3.08 eV for MFU-4 is in reasonable accord with the energy barrier of 2.9 eV determined from the dc conductivity as extracted from the dielectric spectroscopy measurements (Figure 8b).

In the case of Co-MFU-4, the spectrum shows a strong absorption band of the tetrahedrally coordinated Co^{2+} ions, corresponding to transitions within the crystal-field split 3d multiplet, with its maximum at approximately 2.1 eV (= 600 nm).[36] The value of the optical band gap therefore depends on the interpretation of this additional spectral feature. In order to compare the spectral features of Co-MFU-4 to those of MFU-4 one may define the intrinsic optical band gap of the former as given by electronic transitions between ligand-centered molecular orbitals or bands. Accordingly, this leads to a cut-off energy and band gap value of 2.72 eV, which is slightly lower than for MFU-4. The corresponding Tauc plot shown in Figure 10 allows for a more accurate determination. The extrapolation of the found linear region reveals a band gap of about 2.86 eV. Tauc plots (not shown) for the other transition types lead to similar band gap values. Again, arriving at a clear preference for a certain transition type is difficult). For the sharp absorption centered around 2.1 eV (600 nm), which we tentatively assigned to the spin-forbidden metal-centered d-d transitions of tetrahedrally coordinated Co(II) ions, the Tauc plot reveals an alternative band gap value of about 1.87 eV. Interestingly, this value is in very close agreement with the energy barrier of 1.8 eV, determined from the dc conductivity (Figure 8b). Theoretical investigations discussed in the following chapter suggest that these low-energy transitions are related to ligand-to-metal charge-transfer electron transitions, which are spin-allowed and, therefore, can be seen as a means to narrow the intrinsic band gap of Co-MFU-4.

## 2.4. Quantum Mechanical Calculations

In order to glean deeper insights into the different mechanisms by which the electronic energy levels (including band gaps) of MFU-4 compounds can be influenced by different building units, quantum mechanical investigations are mandatory. Periodic models were used to simulate the MFU-4 unit cells (with Zn and Co). In order to choose the appropriate method to calculate accurate band gaps we benchmarked our methods with ZnO and MOF-5 for which experimental data are available. These results are complemented by calculations of discrete clusters (i.e., Kuratowski units, Figure 1) representing appropriate secondary building units of the periodic MFU-4-type frameworks. The purpose of including cluster models here, is to follow the relative shifts and dispersion of electronic energy levels when going from zero dimensional discrete molecular units to three-dimensional periodic frameworks.

Figure 10. Tauc plots for MFU-4 (blue curve) and Co-MFU-4 (red curve) sampled at room temperature assuming a direct (allowed) transition. The dashed lines represent fits of the linear regions.

**ADVANCED
FUNCTIONAL
MATERIALS**

www.afm-journal.de

FULL PAPER

www.MaterialsViews.com

2.4.1. MFU-4 and Co-MFU-4 (Periodic Calculations)

Band gap calculations for MFU-4 (Table S1, Supporting Information) using the GGA functionals (PW91 and PBE) indicate values of 2.53 and 2.52 eV respectively, whilst the hybrid functional HSE gives a value of 3.43 eV. The latter value, which is the most confident value due to the accuracy of HSE, is the closest to the experimentally measured value of 3.08 eV (Figure 10). Considering the extrapolation of the diffuse reflectance data at 0 K (Section 5 in Supporting Information), the diffuse-reflectance measurement gives a band gap of 3.16 eV, in reasonable agreement with the calculated (3.43 eV) value.

Analysis of the density of states (**Figure 11**) indicates a major participation of the atoms from the organic ligand and also the chlorine atoms in the valence band, whilst the conduction band is mainly contributed by atoms from the organic ligand. None of the Zn atoms (neither in octahedral nor in tetrahedral sites) is involved in the valence or conduction bands close to the Fermi energy level.

For the Co-MFU-4 unit cell, a band gap of 2.63 eV is found. The periodic calculation, as in the case of MFU-4 has been carried out with the HSE functional, a cutoff of 450 eV, 700 bands included in the calculation, and one single k-point considered due to the large size of the unit cell (204 atoms and 5305 Å^3).
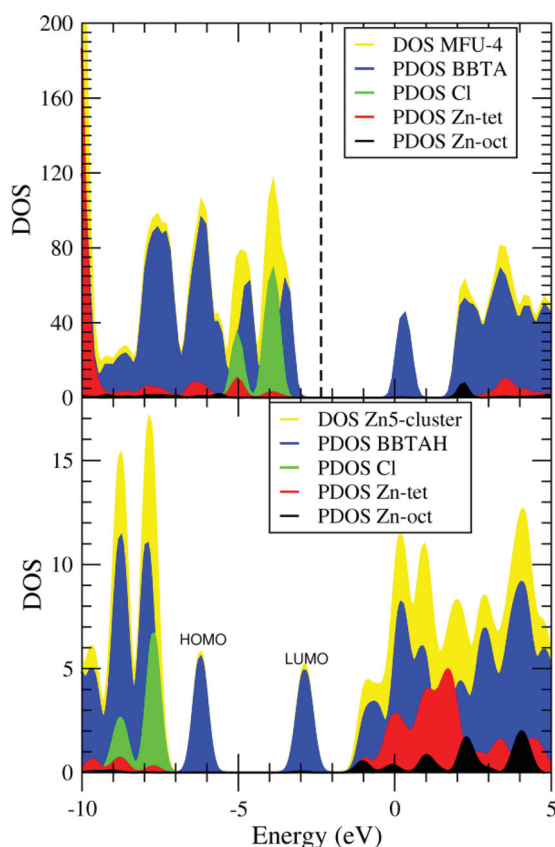
Table 1. Calculated band gaps (eV) for MFU-4 and Co-MFU-4 using HSE functional (periodic and cluster calculations).

	MFU-4	Co-MFU-4
periodic	3.43	2.63
cluster	3.15	2.15
experimental[a]	2.9	1.8
experimental[b]	3.08	1.87 (2.86)

[a]Conductivity studies, cf. Figure 8; [b]Optical spectroscopy, cf. Figure 10.

All Co atoms were considered to be in a high spin configuration. The band gap obtained (2.63 eV) is considerably higher than the experimental value obtained in this work from the diffuse reflectance data (1.87 eV) and from conductivity measurements (1.8 eV; see **Table 1** and Figures 8b,10). Using the extrapolation at 0 K (see Section 5 in Supporting Information) from the diffuse-reflectance data, the experimental value for the band gap is 1.95 eV, slightly closer to the calculated value (2.63 eV) than the value obtained from Figure 8 (1.87 eV). Taking into account the high energy extrapolation at 0 K, the experimental determination, 2.90 eV, would be very close to the calculated. However, from our theoretical analysis we can not establish which of the two assignments (low energy, high energy) should be compared.

As stated in the previous chapter, the main difference with respect to MFU-4 is the participation of occupied and unoccupied Co(3d) orbitals in the valence and conduction bands of the framework close to the Fermi energy level, leading to a significant narrowing of the band gap energy (see **Figure 12** and also supporting information, Figures S7–S9). While the occupied metal-centered orbitals or bands result mainly from the tetrahedrally coordinated Co(II) ions, the energetically low-lying unoccupied electron states, in contrast, are exclusively contributed by the octahedrally coordinated Co(II) ions, which coordinate to the N2 (central nitrogen) atoms of the BBTA ligands.
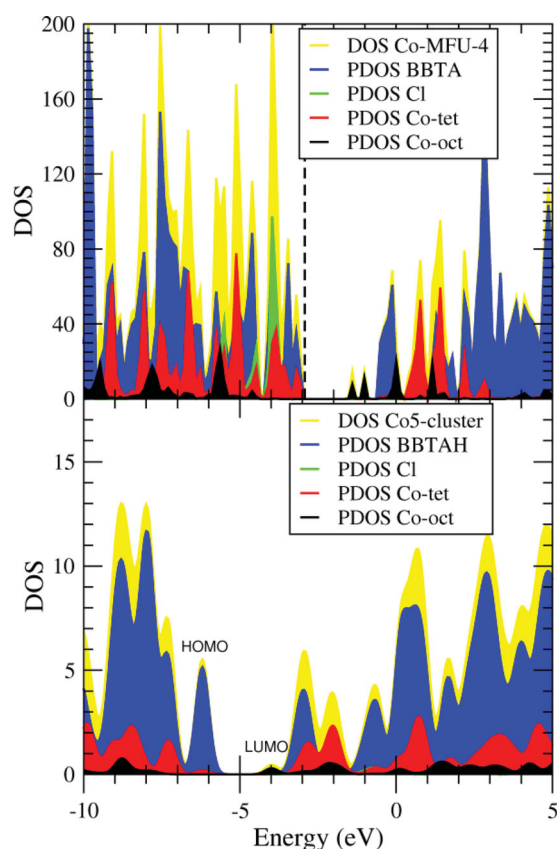
2.4.2. MFU-4 and MFU-4-Co (Cluster Calculations)

Clusters employed in the calculations (M$_5$Cl$_4$(HBBTA)$_6$, with M = Zn^{II},Co^{II}) are shown as Supporting Information (Figure S11).

The result on Zn$_5$Cl$_4$(HBBTA)$_6$ gives a HOMO-LUMO gap of 3.15 eV, very close to the periodic calculated value (3.43 eV). On Co$_5$Cl$_4$(HBBTA)$_6$, three spin states have been taken into account with $S = 1.5$, 4.5 and 7.5, corresponding to 3, 9 and 15 unpaired spins respectively. This depends on how the spins of each Co atom, each of them with a high spin configuration ($S = 1.5$), interact with the spins of the other Co atoms. The latter case corresponds to a ferromagnetic ordering, whilst in the other cases there is less coupling between the spins of adjacent Co atoms. The lowest energy was obtained for the system with the highest spin ($S = 7.5$) which contains 340 alpha-electrons and 325 beta-electrons. The HOMO-LUMO gap is localized in the beta-wavefunctions and it gives a value of 2.15 eV. This value is close to the experimental value (1.87 eV) obtained in this work from the diffuse reflectance data (Figure 10), and also close to the 1.8 eV obtained from conductivity measurements (Figure 8b).

Figure 11. Total and partial density of states (DOS, PDOS) in the periodic (top) and cluster (bottom) calculations of MFU-4. PDOS have been decomposed into the ligand (BBTA), chlorine (Cl), octahedral and tetrahedral Zn atoms. The vertical dashed line indicates the Fermi energy level for MFU-4 at 0 K.

Materials
Views
www.MaterialsViews.com

ADVANCED
FUNCTIONAL
MATERIALS
www.afm-journal.de

An analysis of the molecular orbitals contributes to give an interpretation of the band gap values. First, for the MFU-4 cluster ($Zn_5Cl_4(HBBTA)_6$), all frontier orbitals are mainly participated by the organic ligand (see Supporting Information, Figure S12). This is in agreement with our previous study[37] of the photophysical properties of the MFU-4 related compound [$Zn_5Cl_4(Me_2BTA)_6$], where a band at 282 nm (4.4 eV) was measured in the UV-visible absorption spectrum. This relatively intense band was assigned to the ligand centred $\pi \rightarrow \pi^*$ transition of Me_2BTA^-, and is also present in the molecular compound Me_2BTAH. Previous TD-DFT/HCTH/TZVP calculations, with a result of 4.46 eV, confirmed such assignment and indicated no participation of the metal atoms in the UV/vis spectrum. Interestingly, we have observed decreasing HOMO-LUMO gaps as the conjugation increases in the organic ligand: 1,2,3-triazole (7.03 eV), benzotriazole (4.56 eV), and benzo-bistriazole (3.07 eV), with all molecules corresponding to the N-NH-N-type tautomer. In MFU-4, the periodic calculated band gap (3.43 eV), and the cluster calculated HOMO-LUMO gap (3.15 eV) thus are very much related to the HOMO-LUMO gap of the organic ligand itself, namely benzo-bistriazole (3.07 eV). As said above, the analysis of the orbitals and bands shows a participation dominated by the ligand.

Secondly, for the Co-MFU-4 cluster ($Co_5Cl_4(HBBTA)_6$), the HOMO is very similar to that of MFU-4 cluster, mainly participated by the $HBBTA^-$ ligand, and with the same energy (–6.14 eV in both cases). The main difference arises in the LUMO, which in Co-MFU-4 is contributed by the octahedral Co(3d) and the ligand, giving a smaller energy (–3.99 eV) than in the case of MFU-4 (–2.99 eV) in which only the ligand participates (see **Figure 13** and Supporting Information Figures S12–S14). Hence the reduced band gap of Co-MFU-4 with respect to MFU-4 is due to the effect of the Co(3d) orbitals, which contributes to lower the energy of the conduction band.

It also follows from the results that the main trends of the periodic and cluster calculations are very similar, thus indicating that the conducting properties are mainly due to the chemistry of the Kuratowski units rather than to specific features of the extended solid. The presence of transition metals with appropriate d-orbital energies can contribute to fine tune the HOMO-LUMO gaps and the band gaps of the cluster compounds and the corresponding crystalline framework materials.

3. Conclusion

In summary, the metal-organic frameworks MFU-4 and Co-MFU-4 have been investigated by dielectric spectroscopy and by diffusive reflectance spectroscopy in the UV/vis/NIR
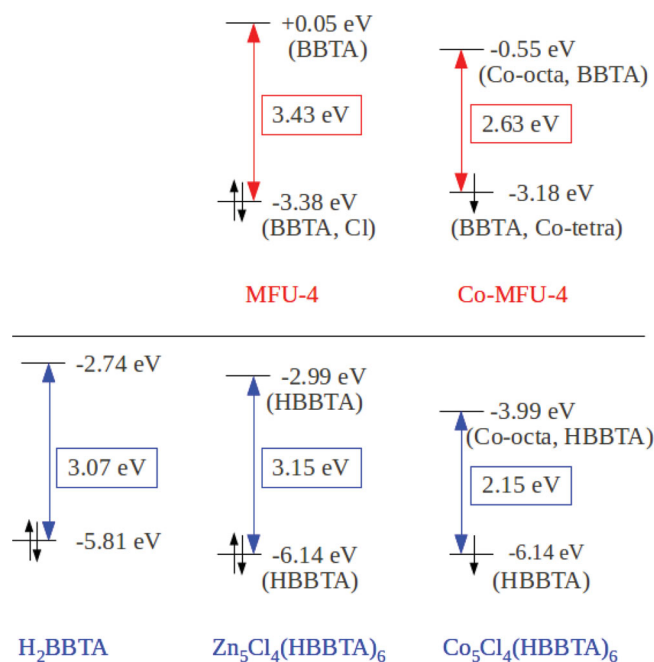

Figure 12. Total and partial density of states (DOS, PDOS) in the periodic (top) and cluster (bottom) calculations of Co-MFU-4. PDOS have been decomposed into the ligand (BBTA), chlorine (Cl), octahedral and tetrahedral Co atoms. The vertical dashed line indicates the Fermi energy level for MFU-4 at 0 K.


Figure 13. Band gaps (top) and HOMO-LUMO gaps (bottom) calculated with HSE functional. Top: Periodic calculations. Bands close to the Fermi energy level are mainly participated by the ligand, except in the case of the conduction band of Co-MFU-4, with a major participation of Co, producing an energy lowering. Bottom: Cluster calculations. In the three cases HOMOs are mainly participated by the ligand. LUMOs of the ligand (left) and MFU-4-cluster (centre) are very similar, whilst in the case of Co-MFU-4-cluster (right), there is a mixture between the ligand and the Co(3d) orbitals, lowering the energy. Details of the orbitals are shown as Supporting Information, Figures S12–S14.

FULL PAPER

region. Dielectric measurements, performed in a broad temperature range (10 to 600 K), have revealed the presence of a variety of relaxational processes in these materials. One of these relaxations (process I) could be unequivocally ascribed to the residual amount of DMF molecules, occluded in the voids of the framework during sample synthesis. These molecules show reorientational motions within the cages of the metal-organic framework. DMF molecules in the bulk show reorientational motions that are much faster than process I (Figure 4) and confinement effects and interactions with the pore walls of the metal-organic framework can be assumed to slow down the DMF molecules. Concerning the microscopic origin of the additional relaxation processes, currently only speculations are possible: Pores filled with less than the maximal packing of six DMF molecules seem to be a reasonable scenario but reorientations of residual water molecules or slow intramolecular modes cannot be excluded. For a final clarification of the complex relaxation dynamics in MFU-4 and Co-MFU-4, further investigations are necessary. In any case, this type of metal-organic framework seems to be an interesting host system for the investigation of molecular dynamics in confined environment, which can reveal, e.g., information on dynamic length scales when approaching the glass transition.[31]

The dielectric measurements, performed on powder samples, also allowed to deduce the dc conductivity in both materials, which is found to be rather low, reaching values of the order of 10^{-14} Ω^{-1} cm^{-1} at temperatures of 480 K (MFU-4) and 400 K (Co-MFU-4). For MFU-4, thermally activated behavior of $\sigma_{dc}(T)$ with an energy barrier of 2.9 eV was found. In contrast, the Co system showed activated charge transport with $E = 1.8$ eV in a limited temperature region only.

The diffusive reflectance measurements in the UV/vis/NIR range, revealed the clear signature of an interband-transition in both materials. Irrespective of the assumed transition type (direct/indirect, allowed/forbidden), band gap energies of the order of 3.08 eV were obtained for MFU-4, whereas the corresponding values for Co-MFU-4 are 1.87 eV or 2.86 eV, depending on the interpretation of the band structure of the latter. A reasonable agreement was found for the experimentally determined band gap values and those predicted from DFT calculations (cf. Table 1). It should be noted that the band gaps in Table 1 were determined at different temperatures (DFT: T = 0 K; reflectance: room temperature; conductivity: around 500 K) However, as the band gaps in intrinsic band semiconductors are only weakly temperature dependent, it is reasonable that the different methods should lead to comparable results, which indeed is the case. This is further corroborated by the results of temperature-dependent band gap measurements as discussed in detail in the Supporting Information (section 5). All these findings indicate that band-conduction is the dominating charge-transport mechanism in MFU-4, similar to conventional semiconductors. The band gap energy (1.8 eV) for Co-MFU-4, deduced from part of its $\sigma_{dc}(T)$ curve only (Figure 5b), is significantly narrowed by replacing diamagnetic Zn(II) by high-spin Co(II) d^7 ions, leading to the introduction of an (empty) d-derived band, reducing the intrinsic band gap of Co-MFU-4.

Based on these results the following trends can be safely predicted in light of engineering the band gap and thus the
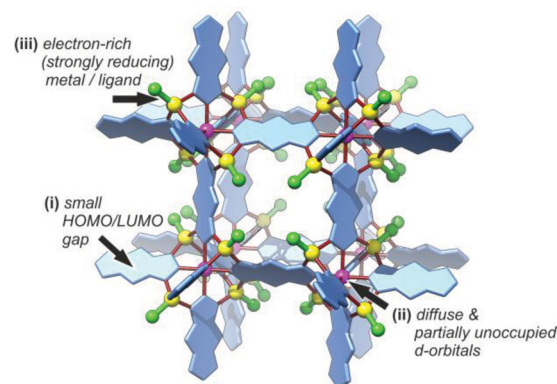
Figure 14. Systematic trends for adjusting the band gap energy in MFU-4-type semiconductors. i) decreasing the HOMO/LUMO gap of the ligand leads to narrow-band gap semiconductors, ii) metal ions in octahedral coordination sites possessing diffuse and partially unoccupied d-orbitals generate empty d-derived bands, iii) metal ions placed in tetrahedral coordination sites generate (partially) filled band states. In all cases the intrinsic band gap is significantly reduced.

technical potential of MFU-4 type semiconducting microporous frameworks (**Figure 14**).

Engineering of the band gap can be done, on the one hand by adjusting the degree of conjugation of the ligand (Figure 14,i), with increasing conjugation leading to higher valence band (HOMO) energy, hence reduced band gap (HOMO-LUMO gap). On the other hand, adjusting the band gap through the energy level in the conduction band seems to be done more efficiently by choosing an appropriate metal whose unoccupied d-orbitals insert below the LUMO energy of the ligand (Figure 14,ii). This is accomplished by octahedral Co(II) ions in Co-MFU-4, which leads to empty d-bands that are by ≈1 eV lower than the lowest lying energy levels of the conduction band in MFU-4. Placing 4d or 5d transition metal ions into the octahedral sites of MFU-4 type frameworks, the energy of the empty d-bands should be shifted to even lower energies, a strategy which we are currently trying to verify experimentally. DFT calculations also suggest that (partially) filled d-bands might be introduced into the band gap of MFU-4 type materials by placing electron rich {metal-ligand} fragments into the tetrahedral coordination sites of the framework (Figure 14,iii). While the current {Zn-Cl} or {Co-Cl} fragments seem to be inefficient in this respect, a host of metal-ligand combinations can be easily introduced into these sites via post-synthetic metathesis reactions,[15,38] rendering the MFU-4 type family of frameworks a versatile construction kit for the design of tailored microporous semiconductors.

4. Experimental Section

Synthesis of Framework Compounds: MFU-4 and Co-MFU-4 were synthesized as described previously.[14,15] The particle size of the obtained powders laid in the range of 2–10 μm. The solvent *N,N*-dimethylformamide (DMF) was removed by heating the samples for 16 h at 280 °C under vacuum. To check for the influence of the solvent, two additional samples of MFU-4 were prepared: One sample was subjected to a higher temperature of 320 °C and another sample was measured as prepared, that is, without removing the DMF.

ADVANCED
FUNCTIONAL
MATERIALS
www.afm-journal.de

www.MaterialsViews.com

FULL PAPER

Optical Spectroscopy: Diffuse reflectance UV/vis/NIR spectra were recorded in the range 300–900 nm using a Perkin Elmer λ 750 s spectrometer and a Labsphere 60 mm RSA ASSY integrating sphere with 0°/d measuring geometry. Labsphere Spectralon SRS-99 was used as a white standard.

Dielectric Spectroscopy: To avoid any pressure-induced deterioration of the sample, all dielectric measurements were performed on powder samples. For this purpose, the powder was filled into a parallel-plate capacitor with an outer support ring made of Teflon, similar to the typical setup used for liquid samples.[39] Only slight pressure was applied to the capacitor plates to ensure a good filling factor. Nevertheless, the absolute values obtained by this method may be somewhat reduced due to a filling factor smaller than unity. After sample preparation and before each dielectric measurement run, all samples were subjected to vacuum for 48 h to remove residual water. The complex dielectric constant ε' and the real part of the conductivity σ' at frequencies 0.01 Hz $\leq v \leq$ 620 kHz were determined using a frequency-response analyzer (Novocontrol α-Analyzer).[39] For sample cooling between 10 and 300 K, a closed-cycle refrigerator was employed. Measurements from room temperature up to 600 K were done in a home-made oven.

Quantum Mechanical Investigations: The periodic calculations on the MFU-4 and Co-MFU-4 unit cells (containing 204 atoms and the chemical composition $4[M_5Cl_4(BBTA)_3]$, with M = Zn,Co) were performed using the VASP.5.2.12 package.[40] VASP evaluates the total energy of periodically repeated geometries, on the basis of DFT and the pseudopotential approximation with the one-electron pseudo-orbitals expanded over a plane-wave basis set. The electron-ion interaction is described by projected augmented waves. The expansion includes all plane-waves whose kinetic energy is below an energy threshold chosen to be 450 eV. These calculations were performed using spin-unrestricted GGA density functional theory, through PW91[41] and PBE[42] exchange correlation functionals (both semilocal functionals), and HSE hybrid functional. HSE has shown its ability to accurately predict semiconductor band gaps, based on the use of a range-separation parameter $w = 0.11$ Bohr^{-1} in HSE06[43] similar to that in accurate TD-DFT PBEh calculations.[44] Cluster calculations were performed with Gaussian09 using Def2-TZVP basis set from Ahlrich's group,[45] and the HSE[46] hybrid functional. The cluster compositions were $M(II)_5Cl_4(H-bbta)_6$ (where BBTA^{2-} is benzo(1,2-*d*:4,5-*d′*)bistriazolate, and M(II) is Zn^{2+} or Co^{2+}), similarly to the MFU-4 material. Following the results with periodic methods in MFU-4 and Co-MFU-4, hybrid functionals were shown to provide the most accurate results. HSE dramatically improves the band gaps relative to the LSDA, the PBE GGA, and the TPSS[47] meta-GGA functionals. The screened exchange approximation appears to be a very powerful tool for density functional treatments of condensed and molecular systems. The discrete energy levels of the molecular orbitals of the clusters have been artificially broadened for the sake of easier comparison with the results of the periodic calculations (Figures 11,12, bottom). The broadening has been made using a gaussian function with 0.5 Ang width at half height using the AOMix software.[48]

Supporting Information

Supporting Information is available from the Wiley Online Library or from the author.

Acknowledgements

[1] M. D. Allendorf, A. Schwartzberg, V. Stavila, A. A. Talin, *Chem. Eur. J.* **2011**, *17*, 11372.

[2] C. Gomes Silva, A. Corma, H. García, *J. Mater. Chem.* **2010**, *20*, 3141.

[3] S.-L. Li, Q. Xu, *Energy Environ. Sci.* **2013**, *6*, 1656.

[4] H. Li, M. Eddaoudi, M. O'Keeffe, O. M. Yaghi, *Nature* **1999**, *402*, 276.

[5] a) B. Civalleri, F. Napoli, Y. Noël, C. Roetti, R. Dovesi, *CrystEngComm* **2006**, *8*, 364; b) L.-M. Yang, P. Vajeeston, P. Ravindran, H Fjellvag, M. Tilset, *Inorg. Chem.* **2010**, *49*, 10283; c) M. Ji, X. Lan, Z. Han, C. Hao, J. Qiu, *Inorg. Chem.* **2012**, *51*, 12389; d) L.-M. Yang, P. Ravindran, P. Vajeeston, S. Svelle, M. Tilset, *Microporous Mesoporous Mater.* **2013**, *175*, 50.

[6] J. H. Choi, Y. J. Choi, J. W. Lee, W. H. Shin, J. K. Kang, *Phys. Chem. Chem. Phys.* **2009**, *11*, 628.

[7] M. Fuentes-Cabrera, D. M. Nicholson, B. G. Sumpter, *J. Chem. Phys.* **2005**, *123*, 124713.

[8] J. H. Choi, H. J. Jeon, K. M. Choi, J. K. Kang, *J. Mater. Chem.* **2012**, *22*, 10144.

[9] a) A. Kuc, A. Enyashin, G. Seifert, *J. Phys. Chem. B* **2007**, *111*, 8179; b) C.-Kai Lin, D. Zhao, W.-Y. Gao, Z. Yang, J. Ye, T. Xu, Q. Ge, S. Ma, D.-J. Liu, *Inorg. Chem.* **2012**, *51*, 9039.

[10] a) L.-M. Yang, P. Ravindran, P. Vajeeston, Mats Tilset, *RSC Adv.* **2012**, *2*, 1618; b) L.-M. Yang, P. Ravindran, P. Vajeeston, M. Tilset, *J. Mater. Chem.* **2012**, *22*, 16324; c) L.-M. Yang, P. Ravindran, M. Tilset, *Inorg. Chem.* **2013**, *52*, 4217.

[11] L. Valenzano, B. Civalleri, S. Chavan, S. Bordiga, M. H. Nilsen, S. Jakobsen, K. P. Lillerud, C. Lamberti, *Chem. Mater.* **2011**, *23*, 1700.

[12] a) S. Takaishi, M. Hosoda, T. Kajiwara, H. Miyasaka, M. Yamashita, Y. Nakanishi, Y. Kitagawa, K. Yamaguchi, A. Kobayashi, H. Kitagawa, *Inorg. Chem.* **2009**, *48*, 9048; b) Y. Kobayashi, B. Jacobs, M. D. Allendorf, J. R. Long, *Chem. Mater.* **2010**, *22*, 4120; c) L. Sun, T. Miyakai, S. Seki, M. Dincă, *J. Am. Chem. Soc.* **2013**, *135*, 8185.

[13] a) S. Patwardhan, A. A. Kocherzhenko, F. C. Grozema, L. D. A. Siebbeles, *J. Phys. Chem. C* **2011**, *115*, 11768; b) F. C. Grozema, L. D. A. Siebbeles, *Int. Rev. Phys. Chem.* **2008**, *27*, 87.

[14] S. Biswas, M. Grzywa, H. P. Nayek, S. Dehnen, I. Senkovska, S. Kaskel, D. Volkmer, *Dalton Trans.* **2009**, *33*, 6487.

[15] D. Denysenko, T. Werner, M. Grzywa, A. Puls, V. Hagen, G. Eickerling, J. Jelic, K. Reuter, D. Volkmer, *Chem. Commun.* **2012**, *48*, 1236.

[16] D. Denysenko, M. Grzywa, M. Tonigold, B. Streppel, I. Krkljus, M. Hirscher, E. Mugnaioli, U. Kolb, J. Hanss, D. Volkmer, *Chem. Eur. J.* **2011**, *17*, 1837.

[17] S. Biswas, M. Tonigold, M. Speldrich, P. Kögerler, M. Weil, D. Volkmer, *Inorg. Chem.* **2010**, *49*, 7424.

[18] In MOF science the term secondary building unit is often employed as a means to describe subfragments of the coordination framework, which appear to be rational from the point of view of the coordination chemist. See the following review: D. J. Tranchemontagne, J. L. Mendoza-Cortés, M. O'Keeffe, O. M. Yaghi, *Chem. Soc. Rev.* **2009**, *38*, 1257. It should be noted that the stringent usage of the term "SBU" in zeolite science has undergone frequent changes in the past. For an insightful discussion on this subject see: N. A. Anurova, V. A. Blatov, G. D. Ilyushin, D. M. Proserpio, *J. Phys. Chem. C* **2010**, *114*, 10160.

[19] a) E. B. Winston, P. J. Lowell, J. Vacek, J. Chocholoušová, J. Michl, J. C. Price, *Phys. Chem. Chem. Phys.* **2008**, *10*, 5188; b) S. Devautour-Vinot, G. Maurin, F. Henn, C. Serre, G. Férey, *Phys. Chem. Chem. Phys.* **2010**, *12*, 12478; c) S. Frunza, A. Schönhals, L. Frunza, P. Ganea, H. Kosslick, J. Harloff, A. Schulz, *J. Phys. Chem. B* **2010**, *114*, 12840; d) S. Devautour-Vinot, G. Maurin, C. Serre, P. Horcajada, D. Paula da Cunha, V. Guillerm, E. de Souza Costa,

F. Taulelle, C. Martineau, *Chem. Mater.* **2012**, *24*, 2168; e) W. Zhang, H.-Y. Ye, R. Graf, H. W. Spiess, Y.-F. Yao, R.-Q. Zhu, R.-G. Xiong, *J. Am. Chem. Soc.* **2013**, *135*, 5230; f) A. B. Cairns, A. L. Goodwin, *Chem. Soc. Rev.* **2013**, *42*, 4881.

[20] F. Kremer, A. Schönhals (Eds.), Broadband Dielectric Spectroscopy, Springer, Berlin, Germany **2002**.

[21] a) A. R. Long, *Adv. Phys.* **1982**, *31*, 553; b) S. R. Elliott, *Adv. Phys.* **1987**, *36*, 135.

[22] It should be noted that the conductivity is related to the dielectric loss ε'' via $\sigma' \propto \varepsilon'' \nu$.[20] Thus, $\varepsilon''(T)$ shows identical behavior as $\sigma'(T)$ (but with different absolute values). Here we prefer the plot of σ' because the offset of the curves, which is caused by the frequency factor, enhances the readability of the graph.

[23] P. Lunkenheimer, U. Schneider, R. Brand, A. Loidl, *Contemp. Phys.* **2000**, *41*, 15.

[24] P. Lunkenheimer, S. Krohns, S. Riegg, S. G. Ebbinghaus, A. Reller, A. Loidl, *Eur. Phys. J. Special Topics* **2010**, *180*, 61.

[25] R. Brand, P. Lunkenheimer, A. Loidl, *J. Chem. Phys.* **2002**, *116*, 10386.

[26] P. Mondal, P. Lunkenheimer, R. Böhmer, A. Loidl, F. Gugenberger, P. Adelmann, C. Meingast, *J. Non-Cryst. Solids* **1994**, *468*, 172.

[27] A. Schönhals, in Broadband Dielectric Spectroscopy (Eds: F. Kremer, A. Schönhals), Springer, Berlin, Germany **2002**, p. 225.

[28] J. Barthel, R. Buchner, B. Wurm, *J. Mol. Liq.* **2002**, *51*, 98.

[29] a) H. Vogel, *Phys. Z.* **1921**, *22*, 645; b) G. S. Fulcher, *J. Am. Ceram. Soc.* **1923**, *8*, 339; c) G. Tammann, W. Hesse, *Z. Anorg. Allg. Chem.* **1926**, *156*, 245.

[30] C. A. Angell, *J. Non-Cryst. Solids* **1988**, *102*, 205.

[31] F. Kremer, A. Huwe, M. Arndt, P. Behrens, W. Schwieger, *J. Phys.: Condens. Matter* **1999**, *11*, A175.

[32] a) M. D. Ediger, C. A. Angell, S. R. Nagel, *J. Phys. Chem.* **1996**, *100*, 13200; b) P. G. Debenedetti, F. H. Stillinger, *Nature* **2001**, *410*, 259.

[33] S. Riniker, A.-P. E. Kunz, W. F. van Gunsteren, *J. Chem. Theory Comput.* **2011**, *7*, 1469.

[34] We also prepared a plot log σ_{dc} vs $1/T^{1/4}$ according to the variable-range hopping model, which, however, also was not able to linearize the complete $\sigma_{dc}(T)$ data.

[35] a) S. M. Sze, K. K. Ng, Physics of Semiconductor Devices, 3rd ed., Wiley-Interscience, Hoboken, NJ, USA **2006**; b) J. Tauc, *Mater. Res. Bull.* **1970**, *5*, 721; c) D. L. Wood, J. Tauc, *Phys. Rev. B* **1972**, *5*, 3144.

[36] A. B. P. Lever, Inorganic electronic spectroscopy, 2nd ed., Elsevier, **1984**, p. 496.

[37] Y.-Y. Liu, M. Grzywa, M. Tonigold, G. Sastre, T. Schüttrigkeit, N. S. Leeson, D. Volkmer, *Dalton Trans.* **2011**, *40*, 5926.

[38] D. Denysenko, M. Grzywa, J. Jelic, K. Reuter, D. Volkmer, *Angew. Chem. Int. Ed.* **2014**.

[39] U. Schneider, P. Lunkenheimer, A. Pimenov, R. Brand, A. Loidl, *Ferroelectrics* **2001**, *249*, 89.

[40] a) G. Kresse, J. Hafner, *Phys. Rev. B* **1993**, *48*, 13115; b) G. Kresse, J. Furthmüller; *Phys. Rev. B* **1996**, *54*, 11169.

[41] J. P. Perdew, Y. Wang, *Phys. Rev. B* **1992**, *45*, 13244.

[42] J. P. Perdew, K. Burke, M. Ernzerhof, *Phys. Rev. Lett.* **1996**, *77*, 3865.

[43] A. Seidl, A. Görling, P. Vogl, J. A. Majewski, M. Levy, *Phys. Rev. B* **1996**, *53*, 3764.

[44] E. N. Brothers, N. Edward, A. F. Izmaylov, J. O. Normand, V. Barone, G. E. Scuseria, *J. Chem. Phys.* **2008**, *129*, 011102.

[45] F. Weigend, R. Ahlrichs, *Phys. Chem. Chem. Phys.* **2005**, *7*, 3297.

[46] J. Heyd, J. E. Peralta, G. E. Scuseria, R. L. Martin, *J. Chem. Phys.* **2005**, *123*, 174101.

[47] J. Tao, J. P. Perdew, V. N. Staroverov, G. E. Scuseria, *Phys. Rev. Lett.* **2003**, *91*, 146401.

[48] a) S. I. Gorelsky, AOMix: Program for Molecular Orbital Analysis, http://www.sg-chem.net/, University of Ottawa, version 6.8, **2013**; b) S. I. Gorelsky, A. B. P. Lever, *J. Organomet. Chem.* **2001**, *635*, 187.